Research Article

David Bischof*, Marco Roth, Fabian Alder, Reto Besserer, Tina Strüning and Markus Michler

Laser micromachining of acoustic chambers for optical microphones

Laserbasierte Herstellung einer akustischen Kammer für ein optisches Mikrofon

https://doi.org/10.1515/teme-2025-0111
Received August 26, 2025; accepted November 4, 2025;
published online January 19, 2026

Abstract: Microphones are essential for voice and sound recognition, yet their dynamic range remains limited compared to the human. This challenge is being addressed by developing an optical microphone based on a vertical external cavity surface-emitting laser (VECSEL). In this work the design and fabrication process of a miniaturized acoustic chamber for such a microphone, using selective laser-induced etching (SLE) in fused silica, is presented. The chamber integrates key functionalities, including precise alignment markers, optical fiber coupling, and thermal and electrical interfaces. The SLE process enables high-resolution 3D microstructuring, supporting compact integration of optical and mechanical components. Experimental results confirm efficient optical coupling and robust structural performance, demonstrating the potential of laser micromachining for next-generation opto-acoustic sensors.

Keywords: selective laser-induced etching; acoustic chamber; microphone

Zusammenfassung: Mikrofone sind essenziell für die Erfassung von Sprache und Geräuschen, doch ihr Dynamikbereich bleibt im Vergleich zum menschlichen Gehör begrenzt. Diese Einschränkung wird durch die Entwicklung eines optischen Mikrofons adressiert, das auf einem vertikal emittierenden Oberflächenlaser mit externem Resonator (VECSEL) basiert. In dieser Arbeit wird der Entwurf sowie der Herstellungsprozess einer miniaturisierten akustischen Kammer für ein solches Mikrofon vorgestellt. Die Kammer wird mittels selektivem laserinduziertem Ätzen (SLE) in Fused Silica gefertigt und integriert zentrale Funktionen wie präzise Ausrichtungsmarkierungen, optische Faserkopplung sowie thermische und elektrische Schnittstellen. Der SLE-Prozess ermöglicht eine hochauflösende 3D-Mikrostrukturierung und erlaubt die kompakte Integration optischer und mechanischer Komponenten. Experimentelle Ergebnisse belegen eine effiziente optische Kopplung und demonstrieren das Potenzial der Lasermikrobearbeitung für die Entwicklung optoakustischer Sensoren der nächsten Generation.

Schlagwörter: Selektives Laserätzen; akustische Kammer; Mikrofon

1 Introduction

Recent advancements in acoustic sensing technologies have been largely driven by the growing demand for audio solutions in portable and consumer devices. A key challenge in this domain is the improvement of the microphone signal, through effective noise suppression to enhance signal-to-noise ratio (SNR). Conventional MEMS-based capacitive microphones are now approaching performance boundaries that limit further noise reduction [1], [2]. As a result, alternative sensing technologies have gained increasing attention, with optical microphones emerging as a promising candidate [3].

This study introduces a concept for a laser-based manufacturing process to fabricate a miniatuized acoustic chamber from glass. These acoustic chambers will serve as a base platform for the integration of customized vertical external cavity surface-emitting laser chips (VECELs) and membranes. The substrates with the acoustic chambers are fabricated using selective laser-induced etching (SLE) and standard metallization techniques. The microphone design

***Corresponding author: David Bischof**, Institute for Microtechnology and Photonics IMP, OST Eastern Switzerland University of Applied Sciences, Buchs (SG), Switzerland, E-mail: david.bischof@ost.ch.
https://orcid.org/0000-0002-3397-0914
Marco Roth, **Fabian Alder**, **Reto Besserer**, **Tina Strüning and Markus Michler**, Institute for Microtechnology and Photonics IMP, OST Eastern Switzerland University of Applied Sciences, Buchs (SG), Switzerland

Open Access. © 2026 the author(s), published by De Gruyter. This work is licensed under the Creative Commons Attribution 4.0 International License.

incorporates several essential functions, including pillars for mounting the VECELs gain chip, an optical entry for sensor readout, electrical circuits for gain chip operation and thermal conductors for effective heat management. The SLE technique allows the development of complex structures for mechanical, fluidic or optical applications [4]–[6]. In this work the SLE process is used to fabricate structures for optimal placement and alignment of the gain chips, membranes and optical measurement channels.

This paper presents the mechanical microphone design, the manufacturing of the acoustic chamber and the characterization of the electrical continuity of conductors and fiber alignment quality.

2 Microphone design

The microphone features a glass-based acoustic chamber, two laser gain chips - one as acoustic sensor and one as reference sensor, and a silicon membrane, as illustrated in Figure 1. The VECSEL gain chips are mounted on a glass pillar, creating a laser cavity in conjunction with the external second mirror on the membrane. These laser chips are thin coupons which are micro-transfer printed onto the pillar of the acoustic chamber. Next, the membrane chips will be actively aligned and assembled on top of the acoustic chamber. Finally, the fiber will be glued into the pillar. The dimensions of the complete microphone are $5 \times 5 \times 1.5\ \mathrm{mm}^3$.

To operate and read out the microphone, the gain chip requires electrical, thermal, and optical interfaces. The electrical interface provides the current necessary for laser pumping and serves as a metallized pathway for thermal management. Effective thermal management is crucial to prevent the laser from overheating and to ensure stable operation.

When an acoustic signal deflects the membrane, it causes a shift in the central wavelength of the laser due to the cavity length change ΔL. This detuning is measured externally by detecting the wavelength shift of the optical signal, necessitating an optical interface. To minimize optical coupling losses, this interface must be positioned very close to the gain chip and is implemented using an optical single-mode fiber connection. This functionality is integrated into the acoustic chamber.

This chamber fulfills several critical functions: it provides a mechanical interface for precise positioning of the gain chip, enables both electrical and thermal connectivity, and facilitates the collection of emitted light. In addition, to enhance the signal-to-noise ratio, the acoustic chamber requires a substantial back volume. Therefore, a 1 mm thick fused silica substrate is employed, which is precisely machined using SLE.

The SLE process uses ultrashort laser pulses that are precisely focused onto a small volume within the micrometer range. The laser treatment alters the glass material, enabling subsequent removal of the modified regions through wet chemical etching with high selectivity. In the case of fused silica, the etching selectivity between unmodified and modified material is approximately 1,000 [7]. By moving or scanning the laser's focal point, known as a voxel, 3D objects can be created. In this study, various structures such as cavities with a depth of 0.8 mm, through-glass holes and pillars equipped with integrated fiber clamps and alignment markers are needed, as illustrated in Figure 2a.

A structured metallization layer is applied to the acoustic chamber, serving as electrical and thermal interface for the gain chip (Figure 2b). The metallized through-glass vias enable current flow into the acoustic chamber and function as a heat sink.

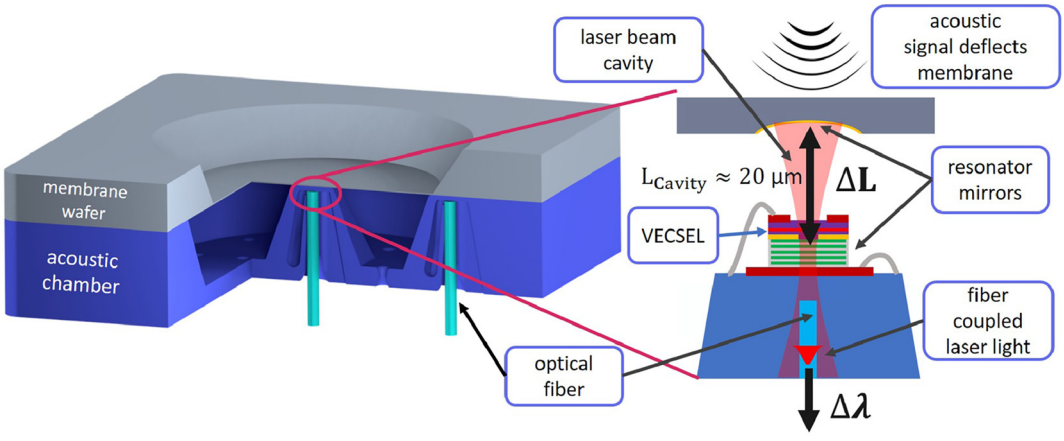
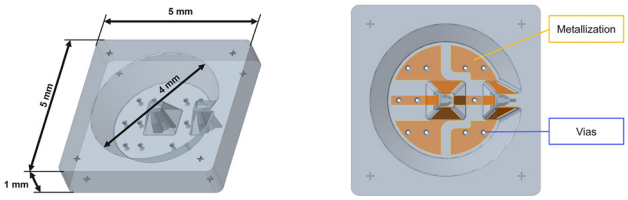


Figure 1: Illustration of the microphone design.



(a) Acoustic chamber glass body (b) Metallized acoustic chamber

Figure 2: Acoustic chamber design of the microphone.

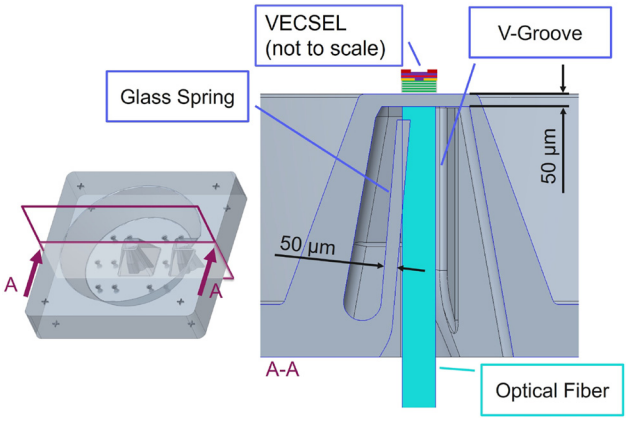


Figure 3: Cross section of the mechanical fiber interface design.

In the optical interface design, a fiber is inserted from the backside of the glass substrate into the pillar (Figure 3). To enhance the positioning accuracy of the fiber, a spring mechanism is employed to push the fiber into a V-groove. This approach allows for a precise alignment, achieving a separation of approximately 50 µm between the fiber facet and the gain chip. By minimizing this distance, optical coupling losses between these components are reduced.

To ensure optimal lateral positioning of the gain chip within the pillars, T-shaped markers are integrated 50 µm below the surface. These subsurface markers are written using laser inscription to avoid etching, thereby preserving the polished surface of the pillar. As shown in Figure 5b, these markers can then be used for precise alignment of the gain chip to the fiber. The key advantage of this strategy is that both the fiber alignment mechanics and the markers are inscribed in the same process step, ensuring high alignment accuracy.

3 Manufacturing process

The manufacturing process of the acoustic chamber involves three steps: three-dimensional bulk micromachining of a fused silica substrate, structured metallization, and optical fiber integration. In Figure 4 the process flow for acoustic chamber manufacturing is visualized.

3.1 Acoustic chamber structuring

3D micromachining of glass is performed by using the SLE process. The laser system operates with a pulse duration of 1 ps, a central wavelength of 1,030 nm, pulse energy of 400 nJ and a repetition rate of 750 kHz. A 20 × microscope objective is used to tightly focus the laser beam, achieving a focal spot in the micrometer range.

The laser focus is scanned across the substrate at a speed of 200 mm/s to define the desired 3D structure within the glass volume. This localized modification alters the chemical reactivity of the material, enabling selective removal in the subsequent etching step.

In the second step, the laser-modified regions are selectively etched using a potassium hydroxide (KOH) solution at 80 °C with a concentration of 8 mol/L. This results in the formation of complex 3D geometries within the glass, as shown in Figure 5.

The root mean square (RMS) roughness of the laser-modified and subsequently etched surfaces typically ranges between 400 nm and 1,000 nm. In contrast, surfaces not exposed to laser treatment – such as the polished top and bottom faces of the substrate – exhibit only minor change in roughness after etching, retaining their original surface quality.

3.2 Metallization of the 3D structure

Following the etching process, the internal surfaces of the structure are coated with a copper seed layer using physical vapor deposition (PVD). A positive photoresist layer is then applied by using spray coating and patterned via shadow-mask photolithography. Due to the chamber's topography - with cavity depths reaching up to 0.8 mm - the resolution of the patterning process within

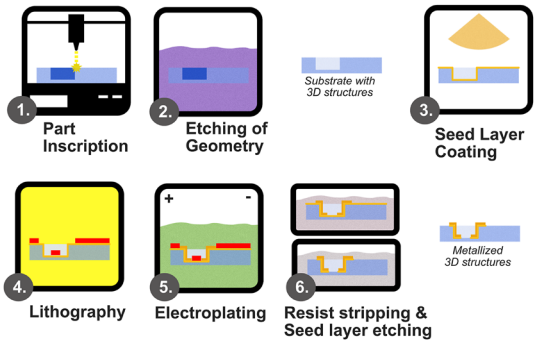
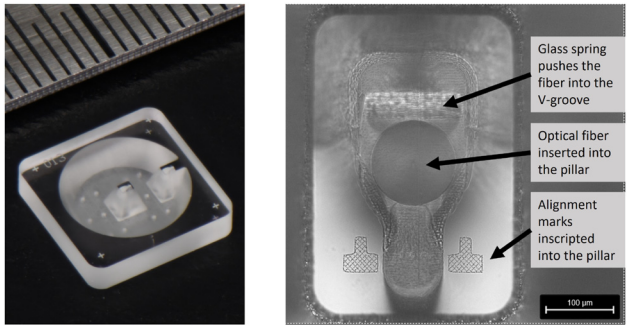


Figure 4: Process flow for acoustic chamber manufacturing.



(a) Glass body (b) Top-view of pillar

Figure 5: Fabricated acoustic chamber.

recessed areas is inherently limited. Therefore, the fidelity of the pattern transfer in these regions must be carefully evaluated.

Subsequently, the exposed areas of the seed layer are selectively thickened through copper electroplating, forming the final thermal and electrical conductive structures.

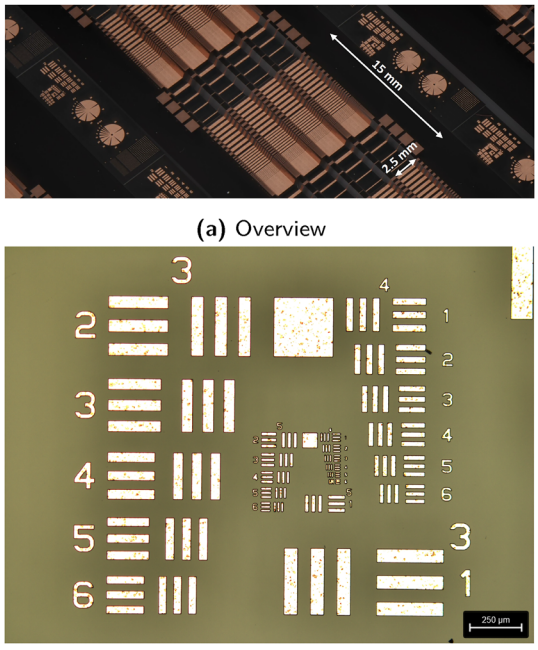
Finally, the photoresist is removed, and the underlying seed layer is selectively etched back to electrically and thermally isolate the resulting metal paths.

The metallization of the acoustic chamber presents specific challenges due to its considerable cavity depth and the inclined geometry of the pillar walls. The increased depth reduces the patterning resolution in the photoresist, primarily because of the greater proximity distance between the lithography mask and the cavity bottom, which limits the size of electrical circuit paths. An example of a metallized test structure is shown in Figure 6. These structures were used to analyze the resolution of the patterning process as a function of cavity depth, d_{cavity}.

The test structure designed for this purpose is presented in Figure 6b. It features a series of parallel lines with defined line widths and equal spacing - commonly referred to as line and space (L-S) patterns. By identifying the point at which adjacent lines and spaces begin to merge, the resolution limit of the patterning process can be determined. The results of this analysis are summarized in Table 1. These values define the design constraints for both the electrical and thermal conduction paths.

Figure 7 shows the metallized acoustic chamber, where the copper coating has been successfully applied to the inclined walls of the pillars, demonstrating effective metallization even on non-planar surfaces.

To evaluate electrical continuity across inclined surfaces, specialized continuity test structures were employed. These structures feature cavities of depth H, with sidewalls inclined at an angle of 30°. Metallization was applied



(a) Overview

(b) Resolution pattern

Figure 6: Copper electroplated test structures.

Table 1: Patterning resolution limit dependence on cavity depth.

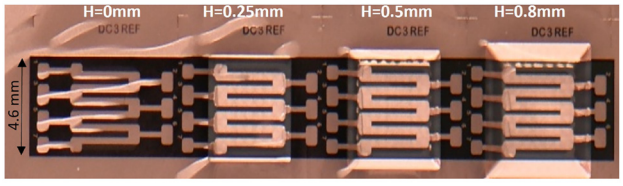
d_{cavity}/mm	$L-S$/µm
0.0	5
0.1	25
0.2	28
0.3	35
0.4	44
0.5	50
0.6	56
0.7	63
0.8	70



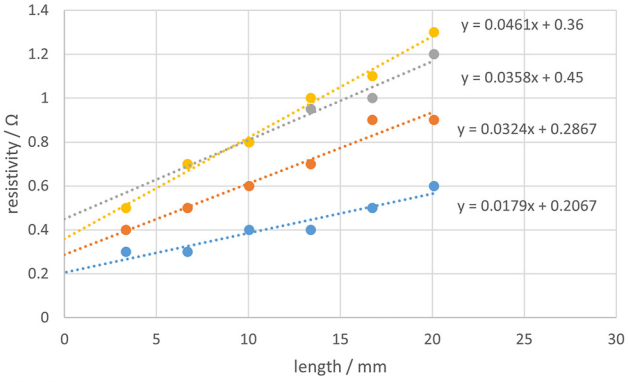
Figure 7: Metallized acoustic chamber.

over this topography. The test circuit includes measurement ports that connect the substrate surface to the bottom of the cavity via the inclined walls. Within the cavity, a meander-shaped conductive path was implemented. Each turn of the meander is equipped with electrical contact points that link back to the substrate surface, enabling localized resistance measurements.

Figure 8a illustrates the layout of the test structures. Using a ohmmeter, resistances were measured between successive ports (e.g., port 1 to 2, 1 to 3, etc.). The results, presented in Figure 8, demonstrate that the structure behaves as an ohmic resistor, confirming the electrical continuity of the metallized inclined walls and the integrity of the meander circuit.



(a) Layout of the meander structure



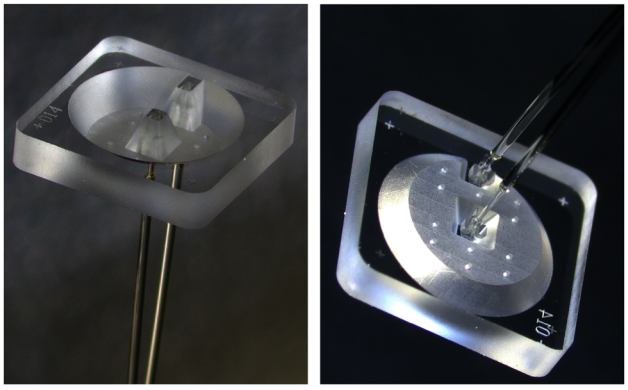
(b) Resistivity measurement result

Figure 8: Meander structure for testing the continuity of the inclined wall coating.

3.3 Fiber assembly

The process starts by stripping the protective coating from the optical single-mode fiber (780HP), followed by thorough cleaning the jacket to ensure a contaminant-free surface. The fiber end is then cleaved to produce a clean, flat facet that is essential for optimal optical coupling.

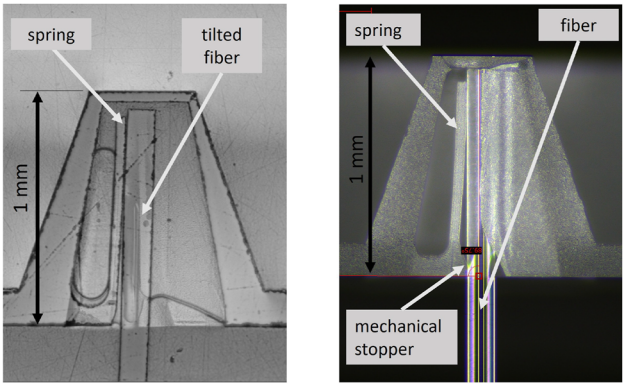
A small droplet of UV-curable optical adhesive (EPOTEK OG198-54) is applied to the fiber tip, which is subsequently inserted into the optical-fiber port of the acoustic chamber. The adhesive fills the gap between the fiber and the 3D glass structure, ensuring mechanical stability. In addition to bonding, the adhesive serves as a refractive index-matching medium, minimizing optical scattering and reflections at the interface between the fiber and the chamber walls. Upon exposure to UV light, the adhesive polymerizes, permanently securing the fiber in place and completing the assembly. The resulting assembly is shown Figure 9.



(a) Front side (b) Back side

Figure 9: Acoustic chamber assembled with fibers. The inserted fiber has a diameter of 125 µm and the glass body has a size of 5 × 5× 1 mm^3.

The fibers are inserted at the rear side of the central pillar as illustrated in the cross-sectional views in Figure 10. In Figure 10a it can be observed that the inserted fiber is tilted, due the clamping close to the fiber facet. As a consequence the fiber is only pushed at the top side into the V-groove. Unfortunately, tilted light coupling into the gain-chips leads to high coupling losses. That is why an additional mechanical stopper was introduced (Figure 10b). By using the later design an angle of 89.7° was measured by microscopy.



(a) Tilted fiber in the design V1 (b) Improved design V2

Figure 10: Fabricated pillar cross-section.

4 Fiber interface characterization

The fiber port must meet two critical requirements. First, it must ensure precise alignment of the fiber core relative to the laser-machined 3D structure of the acoustic chamber. Second, it must enable low-loss optical coupling to the gain chip.

To evaluate the alignment accuracy, the position of the fiber core relative to the internal structures was characterized using microscopy. The pixel resolution of the used microscope configuration was 100 nm per pixel. The resulting measurement uncertainty is in the range of ±500 nm.

Optical coupling efficiency η was assessed via butt-coupling using a second single-mode fiber. The second reference fiber is used to emulate the mode field characteristics of the VECSEL emission. Since the final VECSEL is expected to exhibit a mode field diameter comparable with that of the 780HP fiber, this fiber was selected to characterize the optical interface. The reference fiber, a cleaved bare fiber connected to a 980 nm laser diode, was aligned with the assembled fiber port. The transmitted optical power of the device under test (DUT), denoted as P_{DUT}, was measured using a power meter at the output of the assembled fiber.

To determine the efficiency, a reference measurement was performed by directly coupling two cleaved bare fibers and measuring the transmitted power P_{REF}. The coupling efficiency was then calculated using the following equation:

$$\eta = \frac{P_{\mathrm{DUT}}}{P_{\mathrm{REF}}} \tag{1}$$

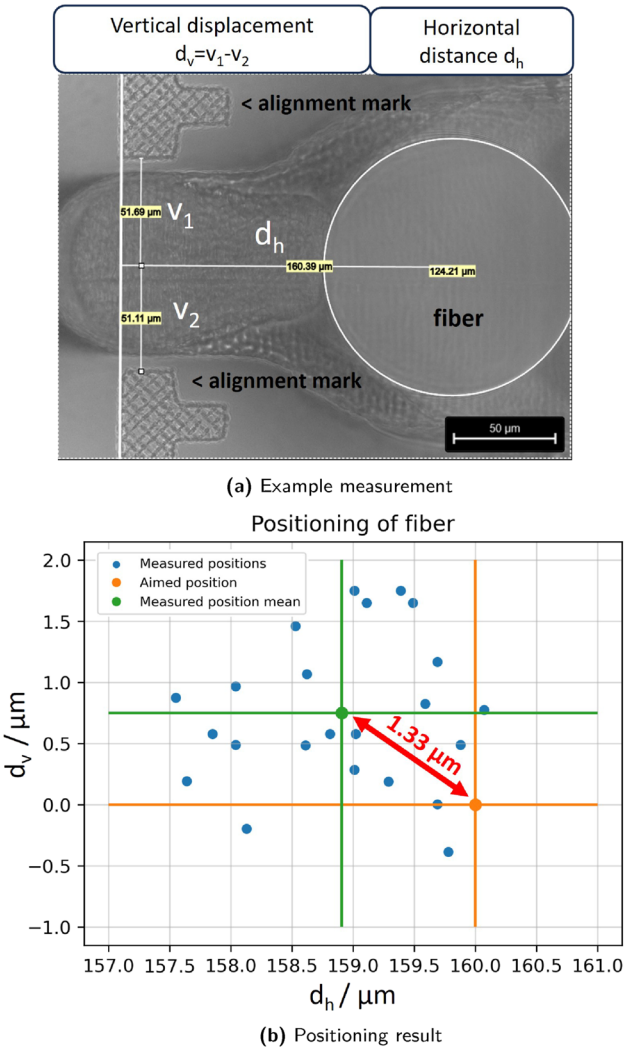
Precise alignment of single-mode fibers is essential to minimize coupling losses. Therefore, a closed-loop controlled XYZ translation piezo stage was employed for fiber positioning. This setup enables systematic investigation of coupling efficiency as a function of misalignment, allowing the definition of alignment tolerances for future packaging of gain chips onto the acoustic chamber. The positioning uncertainty for this setup is in the range of 200 nm.

To minimize reflection losses at the interface between the DUT and the in-coupling fiber, index-matching oil was applied. This reduces Fresnel reflections and scattering at the facet surfaces, thereby improving overall coupling efficiency.

4.1 Fiber positioning

The top view in Figures 5b and 11a reveals that the fiber is clamped against a V-groove. In this view, T-shaped alignment markers are also visible. To evaluate the alignment precision, the position of the fiber cross-section relative to these markers was analyzed using optical microscopy. Two displacement parameters were assessed:

– Horizontal distance (d_{h}): the lateral distance to the T-shaped alignment marks.
– Vertical centering error (d_{v}): the deviation from the vertical center.



(a) Example measurement

(b) Positioning result

Figure 11: Fiber to pillar positioning.

A total of 23 samples were characterized. The resulting deviations are presented in Figure 11b, showing a mean displacement from the target position of 1.33 ± 0.95 µm.

4.2 Fiber coupling efficiency

Using the previously described setup - comprising a translation stage and an in-coupling fiber - the coupling efficiency

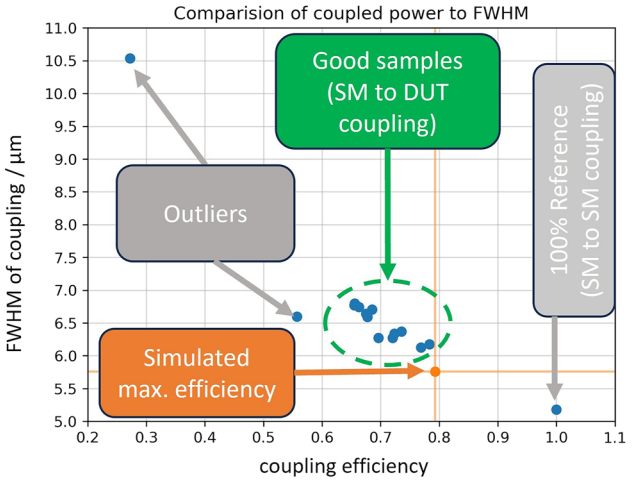


Figure 12: Measured coupling efficiency of the optical fiber interface.

η was characterized. To identify the point of maximum coupling, the in-coupling fiber was scanned laterally until the optical power reached its peak. Subsequently, the fiber was scanned across this optimal position to determine the points at which the coupling efficiency dropped to half of its maximum value.

This full width at half maximum (FWHM) serves as a metric for the required alignment precision between the gain chip and the fiber core of the DUT. The results are presented in Figure 12. In the graph the coupling efficiency is compared with the FWHM. A mean coupling efficiency of 70 % and a FWHM of 6.5 µm were determined.

The coupling efficiency was also investigated through numerical simulations using wave optics propagation methods. For a glass gap of 50 µm, the simulations predicted a theoretical coupling efficiency of approximately 80 %. In comparison, the experimentally measured efficiency was 10 % lower. This discrepancy may be attributed to practical alignment tolerances, surface imperfections, or additional optical losses not accounted in the idealized simulation model.

5 Conclusions

In this study, we successfully fabricated an acoustic glass body for a miniaturized microphone using selective laser-induced etching. The integration of complex 3D structures, including gain chip mounting pillars, optical fiber ports, and alignment markers was achieved with high precision, showcasing the versatility and scalability of the SLE process for advanced micro-optomechanical systems.

The integrated fiber clamp design enabled a coupling efficiency of up to 70 %, with an alignment tolerance of 5 µm, which is a promising result for future packaging of gain chips. The introduction of a mechanical stopper significantly improved fiber alignment, reducing angular deviations and associated optical losses. We were also able to create reliable electrical and thermal connections, even though the deep and sloped surfaces made the metallization process more difficult. The resolution limits of proximity lithography in recessed areas were quantified, providing valuable design constraints for future iterations.

Beyond the technical achievements, this work lays the foundation for the development of high-dynamic-range optical microphones based on VECSEL technology. The demonstrated manufacturing approach is compatible with scalable production and can be adapted for other applications requiring precise metallized 3D structuring in glass.

The results presented here mark a step toward the realization of compact, high-performance optical microphones and open up new possibilities for the use of laser micromachining in miniaturized systems.

Research ethics: Not applicable.
Informed consent: Not applicable.
Author contributions: All authors have accepted responsibility for the entire content of this manuscript and approved its submission. David Bischof: main author, scientific coordinator. Marco Roth: design and structuring of acoustic chambers. Fabian Alder: design, realization and characterization of fiber coupling port. Reto Besserer: metallization of acoustic chambers, Tina Strüning: project management, coating. Markus Michler: supervisor and internal reviewer.
Use of Large Language Models, AI and Machine Learning Tools: Partly used to improve language.
Conflict of interest: All authors state no conflict of interest.
Research funding: This work is funded by the European Union (GA 101129931). Views and opinions expressed are however those of the author(s) only and do not necessarily reflect those of the European Union or European Innovation Council and SMEs Executive Agency (EISMEA). Neither the European Union nor the granting authority can be held responsible for them. Swiss partners in this project are funded by the Swiss State Secretariat for Education, Research, and Innovation (SERI).
Data availability: The raw data can be obtained on request from the corresponding author.

References

[1] A. Gemelli *et al.*, "Recent trends in structures and interfaces of mems transducers for audio applications: A review," *Micromachines*, vol. 14, no. 4, p. 847, 2023.

[2] S. Aisyah Zawawi, A. Azlan Hamzah, B. Y. Majlis, and F. Mohd-Yasin, "A review of mems capacitive microphones," *Micromachines*, vol. 11, no. 5, p. 484, 2020.
[3] N. de Milleri, L. Valli, M. Fueldner, A. Wiesbauer, and A. Baschirotto, "A 22-dba digital optical mems microphone," *IEEE Journal of Solid-State Circuits*, vol. 59, no. 7, pp. 2005—2018, 2024.
[4] Y. Bellouard, "Ultrafast laser to tailor material properties: An enabling tool in advanced three-dimensional micromanufacturing," *Chimia*, vol. 71, no. 5, pp. 295—298, 2017.
[5] D. Bischof, M. Kahl, and M. Michler, "Ultra-short pulse laser-based fabrication process for lightweight structures in quartz glass applied for mirrors," *EPJ Web of Conferences*, vol. 266, p. 3003, 2022.
[6] C. Ross, D. G. MacLachlan, D. Choudhury, and R. R. Thomson, "Towards optical quality micro-optic fabrication by direct laser writing and chemical etching," in *SPIE LASE, SPIE Proceedings*, A. Heisterkamp, P. R. Herman M., M. Meunier, R. Osellame, Eds., SPIE, 2017, page 100940V.
[7] J. Gottmann, M. Hermans, N. Repiev, and J. Ortmann, "Selective laser-induced etching of 3d precision quartz glass components for microfluidic applications — up-scaling of complexity and speed," *Micromachines*, vol. 8, no. 4, p. 110, 2017.